T2: Multi-wavelength diode pumped neodymium doped vanadate lasers

P.K.Mukhopadhyay(pkm@rrcat.gov.in), A.J.Singh, S.K.Sharma and S.M.Oak

I. Introduction:

During the last two decades tremendous progress has been made in diode-pumped Neodymium ion (Nd^{3+}) doped laser systems in terms of efficiency, power and beam quality. However most of the earlier works on diode-pumped Nd:doped lasers focused primarily on the $^4F_{3/2} \rightarrow {}^4I_{11/2}$ transition to obtain lasing at 1.06m wavelength and its intracavity frequency doubling to obtain intense green beam at ~530 nm. Apart from the high gain $^4F_{3/2} \rightarrow {}^4I_{11/2}$ transition, there are other low gain transitions from the sub-levels of $^4F_{3/2}$ to the other levels at $^4I_{9/2}$ and $^4I_{13/2}$ of Nd:doped laser materials [1]. In recent times lots of interest has been generated to exploit these transitions to obtain lasing at ~ 0.9 μm and ~1.3 μm because the intracavity frequency doubling of these wavelengths not only generates radiation in the important blue and red spectral regions but also other useful visible radiations can be obtained by intracavity frequency mixing of these wavelengths. Coherent cw light sources in the visible region are of great importance for a number of scientific and technical applications such as in metrology, remote sensing and medicine etc. [2]. Particularly red, green, and blue (RGB) are the three elemental colors in the visible world, and most visual

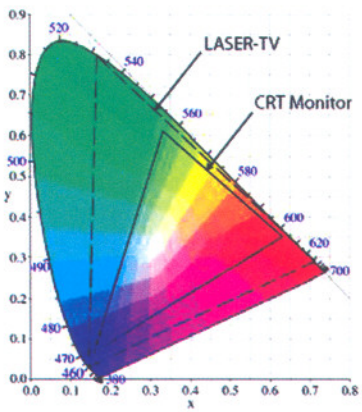

Fig.T.2.1. The CIE 1931 xyY chromaticity diagram The solid triangle represents the chromaticity span of a regular computer monitor, and the dashed triangle represents the chromaticity span of a laser-TV with the primaries λ_B = 458 nm, λ_G = 532 nm and λ_R = 630 nm

colors can be obtained by a weighted combination of these three colors. Hence RGB's three elemental colors can be used in projection displays which have significant advantages over conventional lamp projectors. The superposition of three laser beams with a suitable combination of wavelengths in the red, green, and blue can provide access to a wide color gamut and allows excellent color saturation to be achieved as shown in the chromaticity diagram in Fig.T.2.1. Standard projectors, for instance, can only cover the chromaticities inside the black triangle sketched in Fig.T.2.1. However, with a laser-TV it is possible to obtain a much larger chromaticity span, because the primaries are monochromats situated at the outer border of the chromaticity diagram. Hence, with a laser-TV it would be possible to represent colors in a better way than normal monitors can [3,4] . In addition to laser display, the excellent beam quality from these frequency converted lasers makes it possible to use the individual colors for various applications, for example, green beam for the treatment of diabetic retinopathy, blue beam for undersea communication, red for dermatology etc., are few to mention.

Stimulated emission has been obtained with Nd^{3+} ion incorporated in at least 100 different host materials, but the hosts which are of particular importance for compact RGB sources are vanadate crystals (YVO_4 , $GdVO_4$ etc.) due to their suitability for diode end- pumping and high efficiency.

In this article we describe our studies on diode end-pumped Nd:YVO_4 and Nd:$GdVO_4$ lasers for red, green, blue and yellow beam generation by intracavity frequency doubling and frequency mixing process. Also by combining these two crystals in a single cavity we demonstrate a hybrid laser which is operating at two closely spaced wavelengths which can be a useful source for coherent THz frequency generation.

II. Lasing properties of Nd:doped vanadate crystals:

The energy level diagrams for Nd:YVO_4 and Nd:$GdVO_4$ crystals are shown in Fig.T.2.2. It can be seen that the Nd^{3+} ion has multiple allowed transitions departing from the metastable level $^4F_{3/2}$ to the lower-lying-energy Stark sublevels $^4I_{13/2}$, $^4I_{11/2}$, and $^4I_{9/2}$, leading to potential laser radiations at ~ 1.3, 1.06, and 0.9 μm, respectively. By frequency doubling the lines at these wavelengths we can obtain RGB generation, as several works have reported [5,6]. Above the upper laser level are located the pump bands starting with the manifold $^4F_{5/2}$, which is responsible for absorption around 808 nm. The branching ratios for room temperature fluorescence from the upper laser level to the various manifolds are as follows: $^4F_{3/2} \rightarrow {}^4I_{9/2} = 0.30$, $^4F_{3/2} \rightarrow {}^4I_{11/2} = 0.56$, $^4F_{3/2} \rightarrow {}^4I_{13/2} = 0.14$, and $^4F_{3/2} \rightarrow {}^4I_{15/2} < 0.01$. In Nd^{3+} doped laser material $^4F_{3/2} \rightarrow {}^4I_{11/2}$ transitions producing radiation at ~1.06 μm have the highest emission cross sections (please see table 1). On the other hand the emission cross- sections for transitions, at 0.9 μm and at 1.3 μm, are ~ order of magnitude

lower than that for 1.06 m. To obtain output at these wavelengths, parasitic oscillations at the higher gain transitions should be suppressed sufficiently. Further it can be seen from the Fig.T.2.2 and table-I that Nd:YVO_4 and Nd:$GdVO_4$ has a very similar lasing properties with a slightly different lasing wavelength for a given transition. This enables efficient and controllable dual wavelength operation by combining both the crystals in a single cavity as we will demonstrate in this article. Such sources have potential application for THz frequency generation.

Table I: Properties of Nd:YVO_4 and Nd:$GdVO_4$ crystals

Crystal	Nd:YVO_4	Nd:$GdVO_4$
λ_{em} and σ_{em} for $^4F_{3/2} \rightarrow {}^4I_{11/2}$	1064 nm 15.6×10^{-19} cm^2	1062 nm 7.8×10^{-19} cm^2
λ_{em} and σ_{em} for $^4F_{3/2} \rightarrow {}^4I_{9/2}$	914 nm 0.48×10^{-19} cm^2	912 nm 0.66×10^{-19} cm^2
λ_{em} and σ_{em} for $^4F_{3/2} \rightarrow {}^4I_{13/2}$	1342 nm 0.60×10^{-19} cm^2	1342 nm 0.60×10^{-19} cm^2
Fluorescence lifetime (τ_f)	90μs	90μs
Thermal conductivity	5.1 Wm^{-1}K^{-1}	11.7 Wm^{-1}K^{-1}

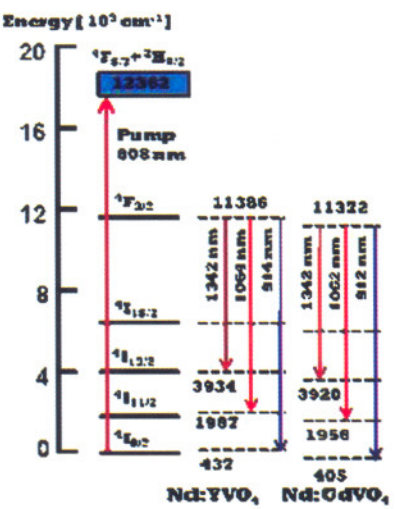

Fig.T.2.2: Energy level diagram of Nd^{3+} doped vanadate crystal . The downward arrows represent the major transitions at 1.06m, 1.3m and 0.9m. The upward arrow represents the pump transition under diode pumping.

Table-II lists the nonlinear crystals used for the intracavity frequency doubling and frequency mixing. For the green and yellow beam generation we used KTP crystal where as for the blue and red beam LBO crystal was used. The crystal and the plane of interaction were chosen considering the phase matching requirements and the effective nonlinearity for the respective frequency conversion process.

Table-II: Nonlinear crystals used for frequency conversions.

Interacting wavelengths (nm)	Crystal Plane	PM angle	d_{eff} (pm/V)
914→457 Type-I	LBOXY	$q=90^0$ $\phi=21.7^0$	0.8
1064→532 Type-II	KTPXY	$q=90^0$ $\phi=23.5^0$	3.58
1342→671 Type-I	LBOXZ	$q=86.1^0$ $\phi=0$	0.82
1064+1342 →593.5 Type-II	KTPXZ $\phi=0^0$	$\theta=78^0$	3.69

III. Operation at ~900 nm and generation of deep blue beam radiation:

The 914-nm emission originates from the $^4F_{3/2}$ manifold and terminates at the highest Stark level of the ground manifold $^4I_{9/2}$ in Nd:YVO_4 crystal. Because the lower laser level is only 437 cm^{-1} above the ground state, there is a significant thermal population in this level at room temperature. This residual population induces a partial reabsorption of the laser radiation which increases the threshold. To achieve a low absorbed pump power at threshold, $P_{a,th}$, one must choose the optimum length L of the active material so the reabsorption losses will be minimal with a significant absorption at the pump beam; these losses are described by the last term in parentheses on the right-hand side of Eq. (1):

$$P_{a,th} = \frac{h\nu_p\left(w_p^2 + w_m^2\right)}{4\sigma\eta_q\left(f_l + f_u\right)\tau}\left(T + 2\alpha_{\text{int}}L + 2\sigma f_l N_{ion}L\right) \qquad (1)$$

where $h\nu_p$ is the energy of a pump photon, w_p and w_m are the radii of the pump beam and the laser mode, respectively, σ is the stimulated-emission cross section, n_q is the pump quantum efficiency, f_l and f_u are the fractional populations of the lower and the upper laser levels, respectively, τ is the fluorescence decay time, T is the transmission of the resonator outcoupling mirror, α_{int} describes the residual internal resonator losses without reabsorption, and N_{ion} is the concentration of doping ions. However the reabsorption term in Eq.(1) is saturable with the intracavity laser intensity at the gain medium. Hence the pump intensity must be scalable for high gain for laser operation well above threshold, as the term for δ_{sat} that describes the saturation of the reabsorption loss approaches zero for high circulating intensities I according to [7]

$$\delta_{sat} = \frac{\sigma f_l N_{ion} L I_{sat}}{I} \ln\left(1 + \frac{2I}{I_{sat}}\right) \qquad (2)$$

where I_{sat} is the saturation intensity given by $I_{sat} = h\nu / [(f_l + f_u)]$ with an energy $h\nu$ of a laser photon. The layout of the compact intracavity doubled Nd:YVO_4/LBO blue laser at 457 nm is shown in Fig.T.2.3.

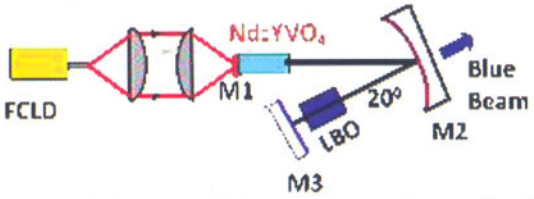

Fig.T.2.3: Schematic of the experimental setup for blue beam generation

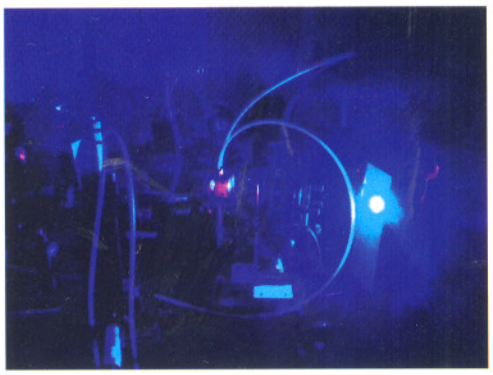

Fig.T.2.4: A photograph of the blue laser under operation.

The pump source is a 30 W 808 nm fiber coupled laser diode array (LDA) with a core diameter of 400 m with 0.22 numerical aperture. The output fiber-tip is reimaged on the gain medium to a spot radius of 200m. We used a 5 mm long a-cut Nd:YVO_4 crystal with 0.1 at% doping concentration as the gain medium. The gain medium was wrapped in indium foil and placed in a water-cooled copper mount. The crystal cooling water temperature was maintained at 10 ^{0}C to reduce the thermal population at the lower laser level. The resonator is a simple three mirror V-shaped cavity designed to obtain a tight spot size at the frequency doubling crystal and a large mode area at the gain medium to obtain a good overlap with the pump beam. The input flat mirror (M1) was highly reflecting (>99.8%) at the lasing wavelength at 914 nm but highly transmitting (>95%) at the pump wavelength at 808 nm. The mirror M1 was directly coated on the front end surface of the crystal. The cavity was folded by a curved mirror (M2) with 50 mm radius of curvature. The end mirror (M3) is again a flat mirror with a dual wavelength high reflection coating at 914 and 457 nm to retro-reflect the backward generated blue beam. The frequency doubling crystal is kept close to M3. The intracavity generated blue beam is taken out through the mirror M2. All the three mirrors are coated for high transmission at 1064 and 1342 nm to avoid the parasitic oscillation at these wavelengths due to their high gain. For intracavity frequency doubling to generate deep blue radiation at 457 nm Type-I critical phase matched LBO crystal (4mm4mm10 mm) is used. The LBO crystal is placed near the mirror M3 to exploit the high intracavity intensity for efficient second harmonic generation.

As the pump power is increased beyond 11W the laser crosses the threshold and intense blue beam is readily observed. In Fig.T.2.5 the slope efficiency curve for the blue beam as well as at the fundamental wavelength is plotted. The operation at 914 nm is obtained in compact plano-concave linear cavity with a curved (100 mm ROC) output mirror with 2% transmission at the lasing wavelength. There are two main characteristics about the output power as a function of input pump power. The first is high lasing threshold (~11 W) and the second is that there is a turning point(~21 W) where the fundamental and 457 nm output power rises rapidly from tens of milliwatts to hundreds of milliwatts. The reasons for these characteristics are all attribute to the saturation of re-absorption loss of the quasi-three-level for fundamental wave 914 nm. At lower pump power, lower circulating intensity exists in the cavity and the corresponding high re-absorption loss leads to high threshold. As the pump power increasing, the circulating intensity becomes so high that it bleaches the re-absorption loss and the output power increases suddenly at this point. The laser will operate like four-level system after this turning point for the re-absorption loss is approaching zero [4]. At the maximum emitted diode pump power of 29 W the CW power at 914 nm and at 457 nm was measured to be 2.3 W and 1.1 W respectively. Around 50% of the generated IR radiation is converted to the blue radiation.

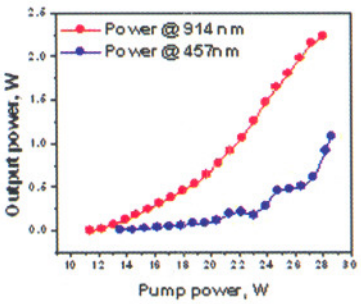

Fig.T.2.5: Slope efficiency curve at 914 nm and intracavity frequency doubled wavelength at 457 nm.

It is worth mentioning here that the doping concentration in the Nd:YVO_4 crystal is an important parameter for CW operation at 914 nm. We observed strong self-pulsing operation with a higher doping concentration such as 0.3at.% doped Nd:YVO_4 crystal as plotted in Fig.T.2.6 due to the saturable reabsorption process. A train of pulses with 150 kHz repetition rate was observed with nearly 100% depth of modulation. The individual pulse duration (FWHM) was ~1μs.

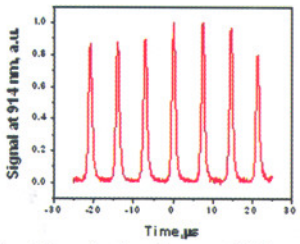

Fig.T.2.6: Self pulsing behaviour at 914 nm with 0.3at.% doped Nd:YVO_4 crystal

IV. Operation at 1064 nm and green beam generation:

Due to the high emission cross-section and four level nature of $^4F_{3/2}$ to $^4I_{11/2}$ transition for lasing at 1064 nm and large effective nonlinearity of the KTP crystal for SHG at 1064 nm we used a compact linear cavity for efficient green beam generation by intracavity frequency doubling as shown in Fig.T.2.7:

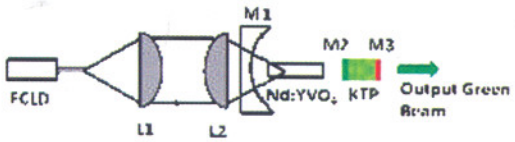

Fig.T.2.7: Schematic of the green laser setup

The input curved mirror M1 (ROC 1 m) was having HR coatings at 1064 nm and HT coating at the pump wavelength at 808 nm. The end mirror M3 is highly reflecting at 1064 nm but highly transmitting at 532 nm and was coated directly on end-face of the KTP crystal. The other face of the KTP crystal was coated HR at 532 nm for retro-reflecting the intracavity generated green beam. The KTP crystal was cut for TypeII phase matching. In Fig.T.2.8 we plot the slope efficiency curve for the green laser along with the measured power at the fundamental wavelength at 1064 nm obtained by replacing the KTP crystal with a flat coupler mirror with 10% transmission at 1064 nm. It can be seen from Fig.T.2.8 that 11W of IR power at 1064 nm was obtain at a pump power of 20 W corresponding to 55% optical to optical conversion efficiency and more than 5 W of CW green beam at 532 nm was obtained at a pump power of ~15W

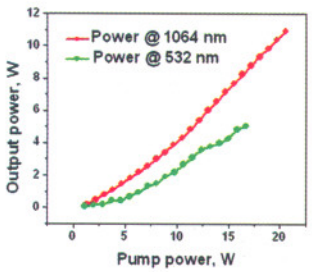

Fig.T.2.8: Slope efficiency curve at 1064 nm and intracavity frequency doubled wavelength at 532 nm

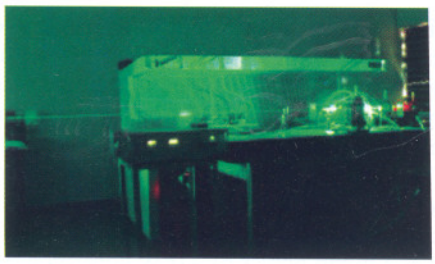

Fig.T.2.9: A photograph of the green laser under operation

corresponding ~ 30% optical to optical conversion efficiency. The output beam is circular in shape with a nearly diffraction limited beam quality (M^2<1.2).

Fig.T.2.10: A photograph of the photocoagulator system based on diode-end-pumped intracavity frequency doubled green laser

The work has been culminated in the development of a green laser photocoagulator for the treatment of diabetic retinopathy as shown in Fig.T.2.10. Green laser beam can reach the eye without much absorption in the intermediate ocular media and get absorbed at the excess blood vessels in the retina of the patients suffering from prolonged diabetes enabling controlled cutting and sealing of these blood vessels.

V. Operation at 1342 nm and red beam generation:

The laser set up for efficient operation at 1342 nm and intracavity frequency doubling for intense red beam generation at 671 nm is same as shown in Fig.T.2.3, only the HR coatings at 914 nm is replaced with that at 1342 nm. For intracavity frequency doubling a LBO crystal was used for type –I phase matching in the XZ plane.

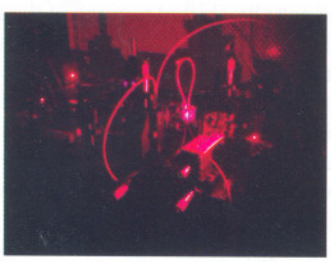

Fig.T.2.11: A photograph of the red laser under operation

In Fig.T.2.12 we plot the slope efficiency curve for the red laser along with the measured power at the fundamental wavelength at 1342 nm obtained in a linear plano-concave cavity with a concave (ROC 100 mm) coupler mirror with 5% transmission at 1342 nm. It can be seen from Fig.T.2.11 that 2.3W of IR power at 1342 nm was obtain at a pump power of 20 W corresponding to 23% optical to optical conversion efficiency and more than 2 W of CW red beam at 671nm was obtained at a pump power of ~16W corresponding ~ 12.5% optical to optical conversion efficiency.

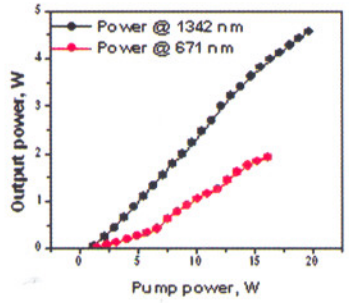

Fig.T.2.12: Slope efficiency curve at 1342 nm and intracavity frequency doubled wavelength at 671 nm

VI. Dual wavelength operation:

Lasers emitting simultaneously at multiple wavelengths can find wide applications in many fields such as environmental monitoring, laser radar, spectral analysis and THz research, etc. In traditional laser systems, however, only one wavelength (or line) operation can normally be obtained if no special measure is taken. The emission lines with weak gain are usually depressed by the line with strong gain because of the gain competition between the laser emission lines, and this competition generally results in only the laser line with the strongest gain being generated. To meet the requirement of simultaneously multiple laser line oscillation, special design of the laser oscillation cavity is necessary to control and to reduce the gain competition among the multiple wavelength lines of the gain medium. The first report about the multiple wavelength laser was presented by Bethea in 1973 by using a Nd:YAG as the gain medium [8]. After that, multiple wavelength lasers based on Nd:YAG[9], Nd:YLF[10], Nd:YVO_4[11] and Nd:CNGG[12] have been reported, by means of designing a typical coating for the output coupler, generating in spatially shifted regions of the gain medium and using two quarter wave plates (QWP) to make the intrinsic frequency split, etc. However, these are not only complex system requiring precise control of the laser and cavity parameters but also suffer from wavelength and power instability due to strong gain competition. Further the power at the individual wavelength cannot be independently controlled due to the fixed relative gain. We have demonstrated a simple laser construction for oscillation at two closely spaced wavelengths by combining Nd:YVO_4 and Nd:$GdVO_4$ crystals in a single cavity. We have earlier seen that for certain transitions these two crystal oscillate with slightly different wavelengths. Hence by pumping both the crystal simultaneously in a single cavity, dual wavelength operation with controllable individual power can easily be obtained. Further Nd:YVO_4 and Nd:$GdVO_4$ being anisotropic crystals with polarized emission the polarization state of the individual wavelength can be varied by changing the relative orientation of the c-axis of these two crystals.

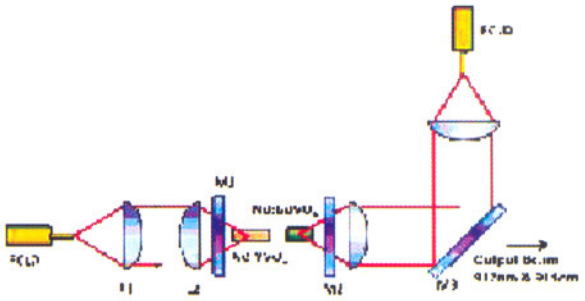

Fig.T.2.13: Schematic of the dual wavelength operation at 914 and 912 nm

The experimental setup for dual wavelength generation at 912 and 914 nm is shown schematically in Fig.T.2.13. A 5 mm long Nd:YVO_4 crystal with 0.3 at.% doping and a 3 mm long Nd:$GdVO_4$ crystal with 0.2at.% doping concentration is inserted in a plane parallel cavity made with two flat mirrors M1 and M2 coated suitably for oscillation at ~900 nm. The crystals are pumped independently by two fiber coupled laser diodes. Both the crystals are placed inside a single water cooled copper block and the temperature of the copper block was maintained at 10 ^{0}C . The output is taken through the mirror M2.

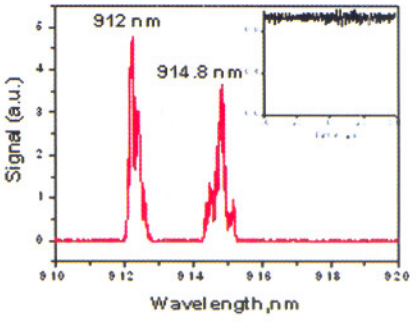

Fig.T.2.14: Recorded spectra from the dual wavelength laser setup. Inset is oscilloscope trace to show the CW operation

The recorded spectrum of the combined output is shown in Fig.T.2.14. It can be seen that the output is oscillating with two distinct wavelengths at 912 and 914.8 nm. The difference

of frequency corresponds to 0.7 THz. The inset of the figure shows the oscilloscope trace of the output power which shows very little temporal modulation though we have used 0.3at.% doped Nd:YVO_4 crystal. This is due to the high intracavity intensity which leads to the bleaching of the population at the lower laser level.

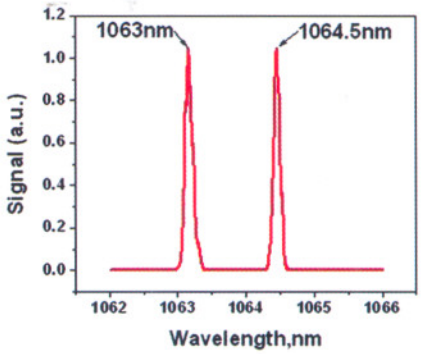

Fig.T.2.15: Dual wavelength operation at 1062 and 1064 nm

In a similar cavity configuration as shown in Fig.T.2.12 dual wavelength operation at 1062.6 nm and at 1064 nm is obtained (Fig.T.2.15) by choosing mirrors with suitable reflectivity. The difference frequency corresponds to 0.3 THz. The total power obtained from this hybrid laser is in excess of 10 W which is divided almost equally to each of the wavelength component. The polarization and power at the individual wavelength can be varied independently by changing the orientation of the crystal and by changing the corresponding diode-pumping power. The flexibility in controlling the parameters of each of the wavelengths makes these sources useful for THz frequency generation.

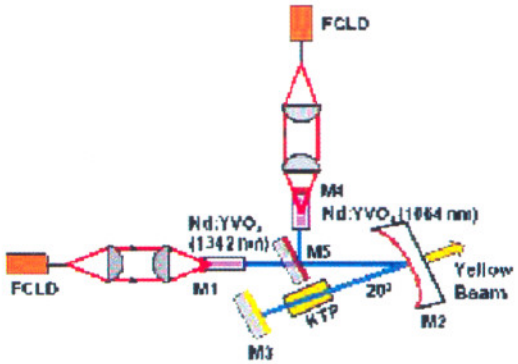

Fig.T.2.16: Schematic of the laser setup for simultaneous lasing at 1064 and 1342 nm and intracavity sum frequency mixing to generate yellow wavelength at 593.5 nm

To generate yellow beam by intracavity sum frequency mixing a simultaneous dual wavelength operation at 1064 nm and 1342 nm is obtained in a combined dual gain dual cavity configuration as shown in Fig.T.2.16. The resonator for oscillation at 1064 nm is made of the mirrors M4, M5, M2 and M3, whereas the mirrors M1, M2 and M3 constitute the resonator for oscillation at 1342 nm. These two resonators are combined to a V-shaped common arm formed by the mirrors M5, M2 and M3, with the help of the mirror M5 which has a high reflection coating at 1064 nm but high transmission coating at 1342 nm. The mirror M3 and M2 are coated highly reflecting for both 1064 nm and 1342 nm and highly transmitting at 593 nm for coupling out the generated yellow beam. Two Nd:YVO_4 crystals are used as the gain media for each of the wavelengths and placed in the respective cavity and pumped separately by laser diodes. Fig.T.2.17 shows the dual wavelength operation at 1064 and 1342 nm.

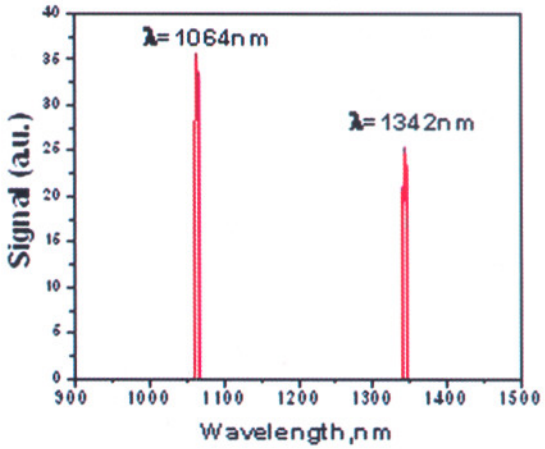

Fig.T.2.17: Dual wavelength operation at 1064 and 1342 nm

For intracavity frequency mixing a type-II phase matched KTP crystal is placed near the mirror M3 of the common arm. As the two wavelengths starts oscillating simultaneously yellow beam is readily observed. A photograph of the yellow laser under operation is shown in Fig.T.2.18.

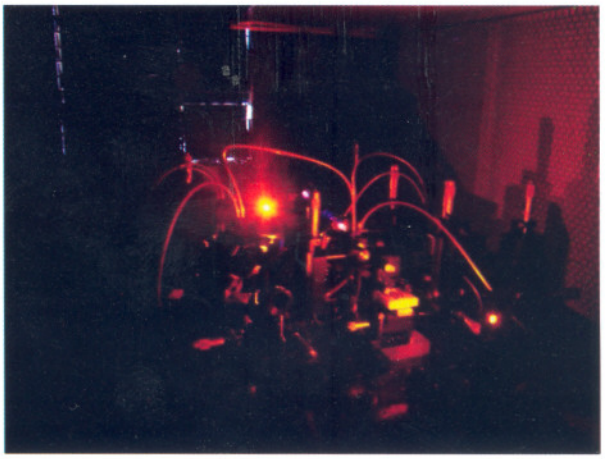

Fig.T.2.18: A photograph of the yellow laser under operation

In Fig. T.2.19(a) we plot the variation of the CW power of the Yellow beam as a function of the total pump power and Fig.T.2.19 (b) shows the wavelength of the generated sum frequency which is at 593.5 nm. The maximum yellow power obtained is ~100 mW.

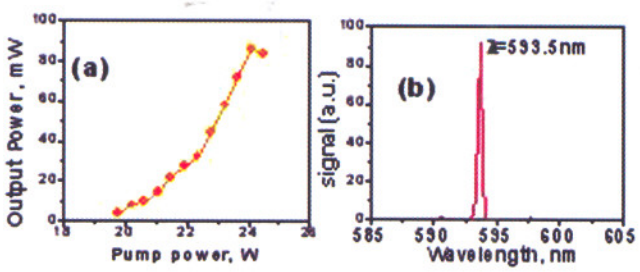

Fig.T.2.19: (a) Variation of generated yellow power as a function of the total pump power. (b) recorded spectra of the yellow laser beam

The reason for the low yellow power is due to the increased intracavity losses as large numbers of intracavity components are used. Further the generated Yellow power becomes unstable at higher pumping power and starts rolling over as the pump power is increased. This could be due to the strong injection of 1064 nm laser beam to the cavity for 1342 nm which disrupts the oscillation at this wavelength.

VII. Summary:

In summary, we have outlined the experimental procedures to generate laser beam at various near infrared as well as in the visible spectral regions by exploiting all the possible transitions in Nd:doped laser material under diode-pumping and given experimental demonstrations using Nd:doped vanadate crystals. It is clear that watt levels of power in the red, blue and green wavelength range can be efficiently generated in a single Nd:doped vanadate crystal which can be efficiently used for laser display or for various medical applications. However due to the homogeneous nature of the transitions and the large differences of gain simultaneous generation of all these colors using a single gain medium is difficult to achieve and lots of efforts are going on this direction. There is also a considerable interest for dual wavelength operation by exciting nearby transitions in a gain medium. In this context we have demonstrated efficient and controllable dual wavelength operation in a hybrid laser incorporating two gain media with slightly different lasing transitions.

References:

1. W.Koechner, Solid-state Laser Engineering, 6th edition, Springer series in Optical sciences, Springer, 2006.
2. H. M. Kretschmann, F. Heine, G. Huber and T. Halldorsson, Opt. Lett. 22, 1461-1463 (1997).
3. Anna Fragemann. Design and construction of a laser display and a new electro-optic modulator. Master's thesis, Lund Institute of Technology, Lund, Sweden, 2001.
4. Edith Innerhofer, Felix Brunner, Sergio V. Marchese, R¨udiger Paschotta, and Ursula Keller. RGB source powers up - laser projection displays. Photonics Spectra, pages 50–54, June 2004.
5. Q. H. Xue, Q. Zheng, Y. K. Bu, F. Q. Jia, and L. S. Qian, Opt. Lett. 31, 1070-1072, (2006).
6. Chenlin Du, Shuangchen Ruan, Yongqin Yu, Feng Zeng, Opt. Exp. 13, 2013-2018, (2005).
7. T. Y. Fan and R. L. Byer, IEEE J. Quantum Electron. QE-23, 605 (1987).
8. C. G. Bethea, IEEE. J. Quantum Electron 9, 254-254 (1973).
9. H. Y. Shen, R. R. Zeng, Y. P. Zhou, G. F. Yu, C. H. Huang, Z. D. Zeng, W. J. Zhang and Q. J. Ye, IEEE. J. Quantum Electron 27, 2315-2318 (1991).
10. H. Y. Zhu, G. Zhang, C. H. Huang, Y. Wei, L. X. Huang, A. H. Li, Z. Q. Chen, Appl. Phys. B 90, 451-454 (2008).
11. Y. Y. Lin, S. Y. Chen, A. C. Chiang, R. Y. Tu, and Y. C. Huang, CW Nd:YVO4 laser, Opt. Express 14, 5329-5334 (2006).
12. H. H. Yu, H. J. Zhang, Z. P. Wang, J. Y. Wang, Y. G. Yu, Z. B. Shi, X. Y. Zhang, and M. H. Jiang, Opt. Lett. 34, 151-153 (2009).